STEPHEN A. MACK, DAVID C. WENSTRAND, JACK CALMAN, and RUSSELL C. BURKHARDT

CHARACTERISTICS OF THERMAL MICROSTRUCTURE IN THE OCEAN

Measurements of ocean microstructure made by vertical profiling and horizontal towing are presented. Emphasis is placed on the geometrical character of microstructure patches and the distribution of these patches with respect to the larger scale temperature and salinity features. The observations are compared with possible physical mechanisms in order to better understand the creation and evolution of the microstructure patches. Vertical profile measurements that reveal microstructure believed to be the signature of salt fingers at temperature-stabilized salinity inversions are reported. Horizontal measurements show patches with similar dimensions (1 to 3 meters high and several hundred meters wide), which are consistent with salt fingers as well as other mechanisms.

INTRODUCTION

The temperature and salinity of seawater are highly variable over the globe and are continuously changing with time at any given place. These variations occur over many different spatial scales (thousands of kilometers to millimeters), time scales (thousands of years to seconds), and magnitudes (tens of degrees to millidegrees, tens of parts per thousand to parts per hundred thousand). These differences in temperature and salinity are distributed by ocean currents that themselves are also highly variable, with comparable time and space scales and with magnitudes ranging from zero to several meters per second. Because of the complex interactions of the ocean with the atmosphere (as influenced by weather systems and by seasonal and diurnal effects), coastal effects, and tides, the ocean is constantly being agitated and never reaches a steady state. As different water masses move and come in contact with each other, mixing occurs. One of the objectives of oceanographers is to learn how much mixing occurs, where and when, with what intensity, and on what spatial and temporal scales.

The signatures of mixing in the ocean are small-scale temperature and salinity fluctuations. The smallest scales are limited by the molecular diffusion of heat and salt as described by the general diffusion equation,

$$\frac{\partial q}{\partial t} = K\nabla^2 q \,, \qquad (1)$$

where q is the quantity being diffused and K is the corresponding molecular diffusivity. The molecular diffusivity of heat ($K_T \approx 1.5 \times 10^{-3}$ square centimeter per second) is two orders of magnitude greater than that of salt ($K_S \approx 1.3 \times 10^{-5}$ square centimeter per second); thus, sharp temperature structures can be expected to diffuse away significantly faster than salinity structures. If a mixing event were to create an infinitely sharp step-like feature in temperature and salinity, then, because of the two orders of magnitude difference in the diffusivities, the temperature feature would have diffused to about 1 centimeter in thickness in 3 minutes, whereas the salinity feature would be only 1 millimeter thick at the end of that same period. Ocean structures from these smallest scales to about 0.5 to 1 meter have been labeled "microstructure." This microstructure has been observed under many different conditions: e.g., underneath Arctic ice,[1] at the bottom of the Red Sea,[2] in the Mediterranean outflow,[3] and in the main thermocline.[4] The fact that microstructure is found in so many places under such different conditions implies that there are many mechanisms for its generation.

GENERATING MECHANISMS

Many of the mechanisms for generating microstructure are discussed at length in the book by Turner[5] and in a review article by Gregg and Briscoe.[6] Some of the hydrodynamic mechanisms are briefly reviewed here.

Double Diffusive Instabilities

If hot salty water lies above cold fresh water, an instability can result even if the denser fluid is underneath lighter fluid. The instability results from the fact that heat and salt diffuse at different rates. The source of energy is the potential energy in the salt gradient; the effect of the instability is to transfer salt downward, which lowers the center of gravity. As shown in Fig. 1, a particle of water that is perturbed, say, upward, soon warms to the temperature of the surrounding water yet retains its lower salt concentration. It is, therefore, lighter than the surrounding fluid and continues to rise. Similarly, if a particle is perturbed downward, it soon cools; but it is more dense than the surrounding fluid because of its higher salinity, so it continues to sink. In the laboratory, long thin columns of cells called salt fingers appear.

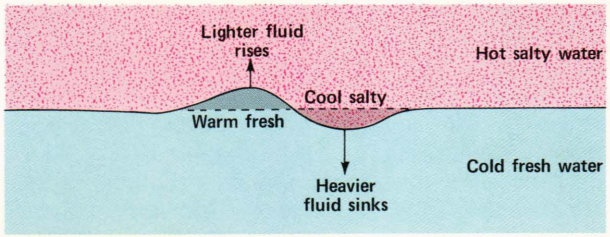

Figure 1 — Diagram of salt-finger instability. A faster transfer of heat than of salt in a perturbed interface of hot salty water overlying cold fresh water creates "blobs" of relatively light and heavy fluid that rise and sink. In the laboratory, long thin columns of cells called salt fingers appear.

Limited ocean observations of salt fingers have been made[7,8] in such localized regions as the Mediterranean outflow. Schmitt and Evans[9] propose that salt fingers should be nearly ubiquitous in much of the ocean thermocline but that their small-scale nature has thwarted their observation by all but very specialized high-resolution sensors. A related instability occurs if the hot salty water is under the cold fresh water. With the density still increasing downward, an instability develops that takes the form of a growing oscillation. The oscillation grows to a certain amplitude, and a series of small layers can result. A detailed stability analysis shows the relationship between the magnitudes of the temperature and salinity gradients and the diffusivities of heat and salt required for the different instabilities. Much research has been devoted to the problem of finding the wavelengths, growth rates, layer formation, horizontal variations, stability, and heat and salt transports of the salt fingers.

Another double diffusive instability that gives rise to small layers results from the difference between the diffusion of salt (or heat) and the momentum in stratified geostrophic shear flows. In a geostrophic shear flow, isopycnals (constant density surfaces) are tilted; the balance of forces is between pressure gradient and Coriolis force in the horizontal and between pressure gradient and net gravitational force in the vertical. If the momentum and salinity diffusivities are different, this balance is upset and the motion is unstable. In the laboratory, the finite amplitude effect is a series of layers.[10] Although this mechanism may be occurring in the ocean,[11] it has not been verified, perhaps because of the difficulty of making the appropriate measurements.

Shear Instabilities

A flag flapping in the wind is a simple example of a shear instability. A related instability can occur in the ocean when the currents have spatial gradients, most commonly in the vertical. A dramatic laboratory demonstration of this instability is easily obtained by placing two fluids of different density, one of them colored by dye, in a narrow, closed rectangular box. As shown schematically in Fig. 2, when the box is tilted, the heavier fluid rushes toward the bottom and the lighter fluid toward the top, creating an intense shear across the interface. The interface "rolls up" in a familiar billow pattern. This characteristic overturning is seen in certain cloud formations and has been observed in the ocean as well.[12] The overturning spirals eventually mix up the water, and a characteristic layer can result if the water is stratified. One of the interesting characteristics of this instability is that the vertical scale is determined by the height of the shear region, so that the resulting layers can occur over a variety of length scales. In particular, small-scale (centimeter) layers result from shears acting over small vertical extents. The shear can result, for instance, from interleaving currents, large internal waves, or boundary effects. In addition, internal waves can break, creating mixed regions of yet another origin.

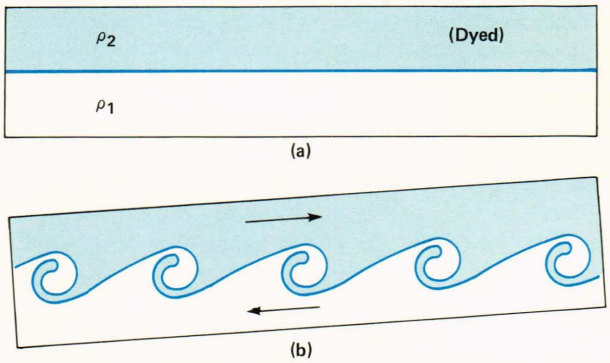

Figure 2 — Diagram of shear instability. (a) Two fluids at rest in a narrow, closed rectangular box. The lighter fluid, ρ_2, is dyed. (b) When the box is tilted, the heavier fluid rushes toward the bottom and the lighter fluid toward the top, creating an intense shear across the interface. The interface "rolls up" in a billow pattern, and the overturning spirals eventually mix up the water.

Complications

Although theoretical studies of small-scale instabilities are quite extensive, and although beautiful laboratory demonstrations of their existence are readily available, observing them in the field and determining their actual role in the overall scheme of oceanic mixing is quite difficult. The difficulty arises because of serious complications resulting from many other effects. Conditions for the small-scale instabilities arise from motions at all larger scales. The interaction of currents, waves, boundaries, and other instabilities of all different sorts and sizes makes the occurrence of microstructure intermittent in space and time.

In order to understand the variety of mechanisms responsible for microstructure in the ocean, measurement systems at APL have been deployed to probe the ocean both in the vertical and in the horizontal. The requirements for such measurement systems include the ability to detect the centimeter-scale temperature fluctuations, to measure the horizontal and vertical extent of the microstructure, and to measure the larger scale ocean features in which the microstructure is embedded. In the remaining sections, two systems currently used to measure microstructure are

briefly described, examples of microstructure observations are given, and possible generating mechanisms are discussed.

VERTICAL MEASUREMENTS OF OCEAN MICROSTRUCTURE

Vertical measurements of temperature microstructure have been made with a modified conductivity, temperature, and depth (CTD) instrument system from Neil Brown Instruments Systems, Inc. (NBIS), lowered from a ship with a winch. The standard CTD system has been modified in several ways so that small-scale temperature and salinity measurements have been optimized. A separately digitized Thermometrics P85 fast-response thermistor has been used rather than the combination thermistor and platinum thermometer pair in the standard CTD system. The P85 thermistor has a time constant on the order of 8 to 10 milliseconds at a drop speed of 1 meter per second. The conductivity is measured with a standard 3-centimeter-long NBIS rectangular conductivity cell. The conductivity cell measures a spatially averaged conductivity over a vertical length slightly greater than the actual cell length. Its frequency response has a form

$$|H(k)|^2 = \left[\frac{\sin(kl/2)}{kl/2}\right]^2, \qquad (2)$$

where k is the radian wave number and l is the effective averaging length. This function is less than 3 decibels below unity (that is, greater than half power) for wavelengths greater than 8 centimeters. This spatially limited response is similar to the thermally limited thermistor response and leads to separate measurements of temperature and conductivity, which can be used to compute salinity and density with a minimum of either noise or the so-called salinity spikes that are created when temperature and conductivity responses are not well matched.

In addition to these modifications, a fluorometer designed and built at APL[13] has been added to the system. This sensor measures fluorescent dye concentration and makes the system useful for repeated measurements over a given water mass that has been tagged with dye. The system is thus also useful for studies of waste disposal and power plant or river outflow. Figure 3 shows the combined CTD and fluorometer system, as well as a close-up of the temperature and conductivity sensors. All sensor channels are sampled at 50 hertz, giving a vertical sample every

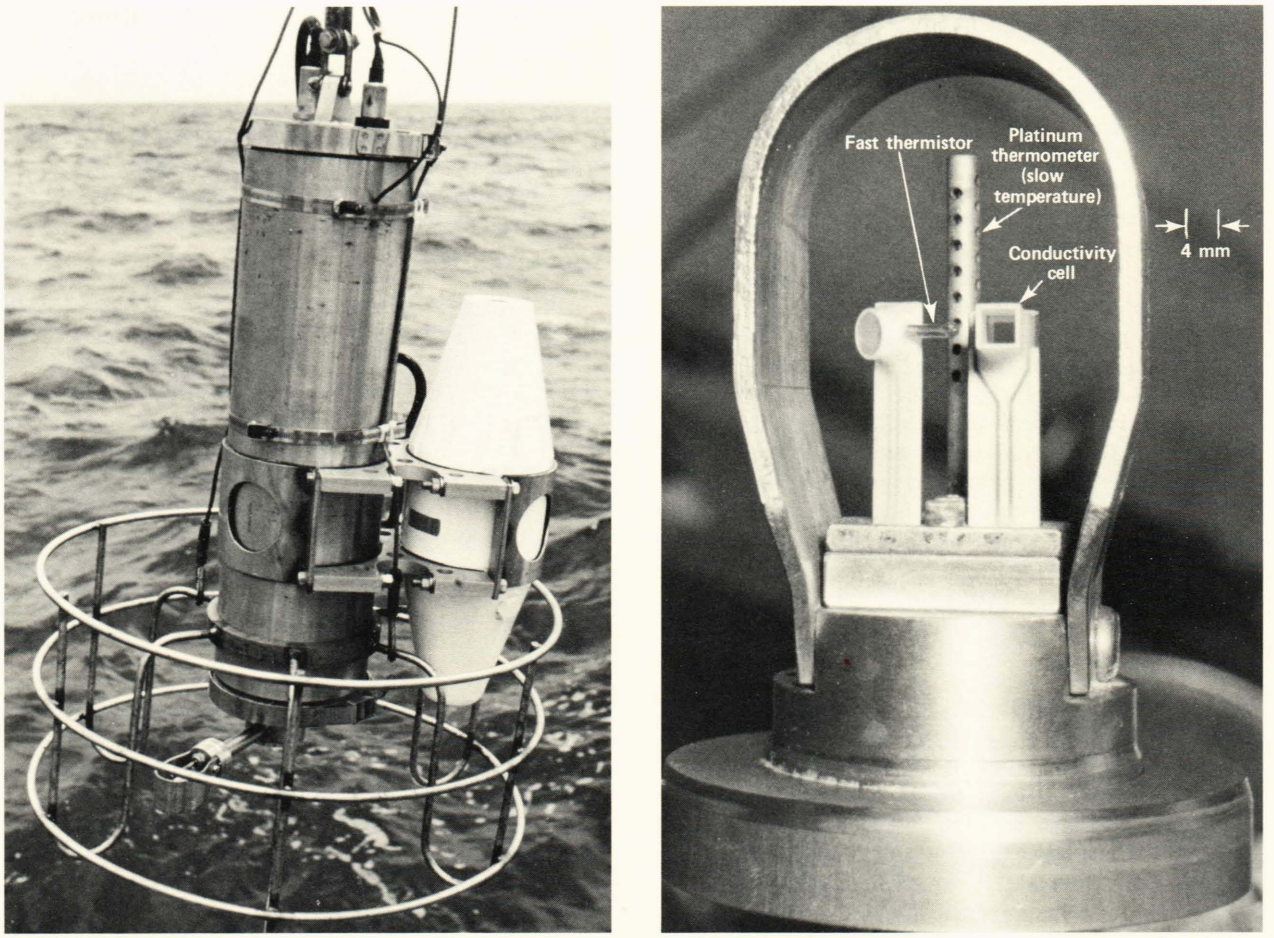

Figure 3 — CTD fluorometer system used for vertical profiling. The underwater unit is at left, and at right is an enlarged view of the sensor arm.

2 centimeters at a typical drop rate of 1 meter per second.

Figure 4 shows a 200-meter vertical profile taken at the Tongue of the Ocean near Andros Island in the Bahamas. Temperature, salinity, and density (plotted as the density function $\sigma_t = (\rho - 1) \times 10^3$, where ρ is the density in grams per cubic centimeter) are plotted against depth in meters. This profile identifies regions of the upper 200 meters that might be suitable for various mixing mechanisms. The surface mixed layer extends to about 55 meters. Below this depth, the temperature and σ_t gradients increase and show a wealth of several-meter-scale structure called fine-structure. The salinity profile shows several large-scale inversions; however, the magnitude of these inversions is small compared with the negative temperature gradients, resulting in a density profile that increases with depth and is thus stable.

In order to investigate the centimeter-scale temperature microstructure and to observe the horizontal extent of any microstructure patches, the CTD underwater unit was repeatedly lowered and raised in the depth range from 110 to 140 meters, a region that shows many salinity inversions. This yo-yo mode of operation was carried on while the ship was drifting with respect to ground at a speed of approximately 20 meters per minute. During this time the surface sea state was calm and the sensor descent rate was uniform. The data taken during the descent of each yo-yo have been plotted in a waterfall fashion in Fig. 5.

The three plots are temperature, salinity, and temperature gradient profiles. The scale at the bottom of each plot represents the scale for the first profile. The time for the start of each profile is shown by a light line drawn to the time axis at the top. Because of the ship drift, each minute of time represents a horizontal distance of about 20 meters. The extent of these measurements is, therefore, 30 meters in the vertical and about 200 meters in the horizontal. The temperature profiles show many small-scale inversions near 130 meters and a strong gradient feature at 135 meters. The salinity profiles indicate that, indeed, the temperature and conductivity sensor responses are well matched, as shown by the absence of salinity spiking at 135 meters, the location of the sharpest

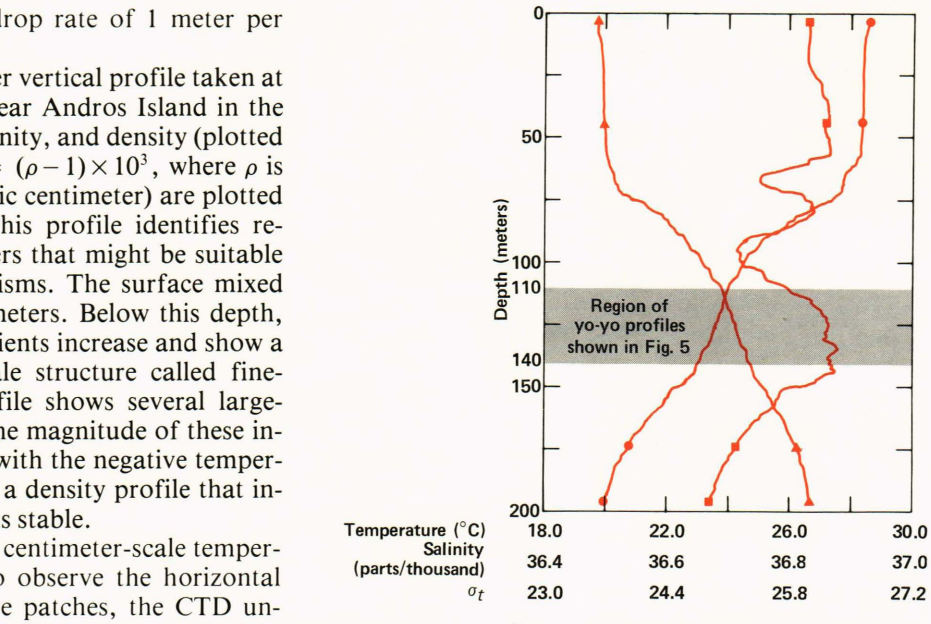

Figure 4 — Vertical profiles of temperature, salinity, and the density function σ_t ($\sigma_t = (\rho - 1) \times 10^3$, where ρ is density in grams per cubic centimeter) taken in the Tongue of the Ocean, Bahamas. The 30-meter region between depths of 110 and 140 meters was chosen for repeated vertical yo-yo measurements while the ship was drifting. An enlargement of this region is shown in Fig. 5.

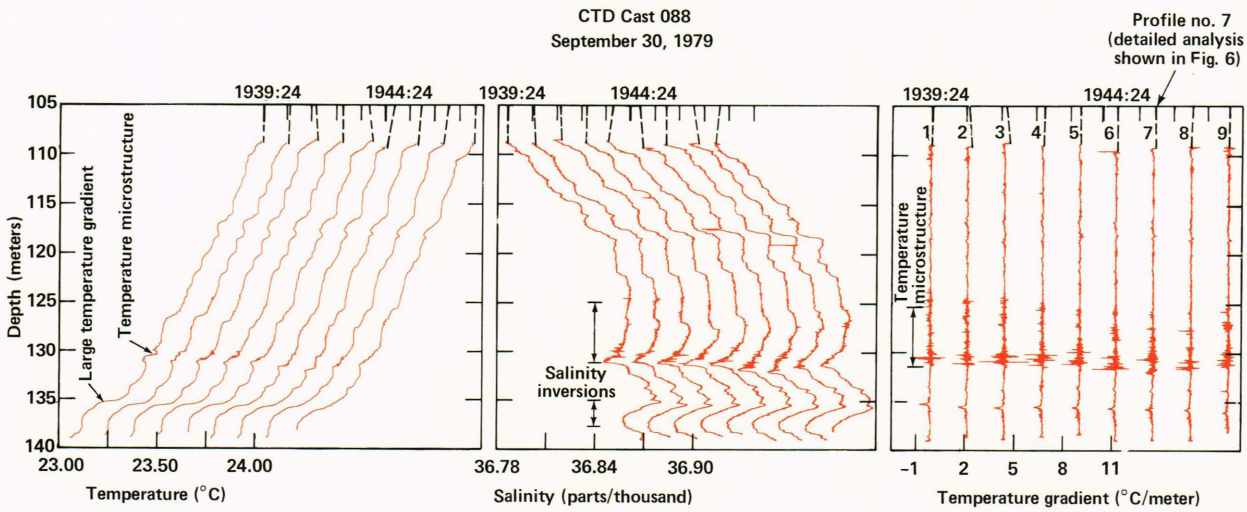

Figure 5 — Series of vertical profiles of temperature, salinity, and temperature gradient resulting from repeated yo-yo measurements of the CTD fluorometer system over the 30-meter vertical extent seen in Fig. 4. These profiles were begun just a few minutes after completion of the 200-meter profile shown in Fig. 4. As a result of surface ship drift, the horizontal extent of the measurements is approximately 200 meters. The microstructure seen near 130 meters in the temperature and salinity profiles is visually enhanced in the temperature gradient plot. The salinity inversions represent potential sites of salt fingers. (The scale at the bottom of each plot is for the first profile.)

temperature feature. Further, these salinity profiles show two regions of salinity inversions, one between 125 and 131 meters and another between 135 and 137 meters. The temperature gradient plot enhances the smallest scale temperature microstructure. Increased microstructure is observed between 125 and 131 meters, with the strongest signal appearing between 129 and 131 meters. These depth regions are coincident with a salinity inversion, thereby creating the condition necessary for salt fingering: hot salty water overlying cold fresh water.

Linear stability analysis and laboratory tank studies[5] predict that salt fingers can occur when the stability parameter, defined as the ratio of the temperature contribution to density ($\alpha\Delta T$, where $\alpha = -(1/\rho)(\partial\rho/\partial T)|_{S,P}$) to the salinity contribution to density ($\beta\Delta S$, where $\beta = (1/\rho)(\partial\rho/\partial S)|_{T,P}$), is less than the ratio of the molecular diffusivities of temperature (K_T) and salinity (K_S); that is, $\alpha\Delta T/\beta\Delta S$ is less than K_T/K_S, which is about 100. Furthermore, Schmitt and Evans[9] predict that salt fingers are highly likely as this ratio approaches unity.

Our fine-scale measurements of both temperature and salinity permit an accurate determination of this stability ratio and, thus, a test of these predictions. Figure 6 shows this determination for profile number 7 of Fig. 5. The temperature gradient is replotted in the left-most panel. A running least-square fitting algorithm has been used over 101 points (about 2 meters) to compute the smoothed temperature and salinity gradients (shown in the next two panels), and those gradients have been combined to form smoothed values of the stability ratio $\alpha\Delta T/\beta\Delta S$ (shown in the fourth panel). The stability ratio is plotted from values of -9 to $+9$. Negative values of this ratio that result from negative temperature gradients and positive salinity gradients represent stable temperature and salinity contributions to density. The region of intense microstructure (between about 127 and 131 meters) is characterized by positive stability parameter values between $+1$ and $+2$, which are in agreement with predictions for salt fingers. This water structure presents very strong evidence of conditions that would support the salt-finger mechanism.

Figure 6 further indicates that, although similar values of this ratio are observed at 136 meters, no microstructure was measured. It may be that the critical value for the onset of salt fingering has not yet been reached at this depth. With further molecular diffusion, this temperature gradient will be reduced faster than the salinity gradient, thereby reducing the stability ratio and perhaps causing the onset of salt fingering. The salt-finger mechanism would then transfer salt faster than heat between depths and would eventually smooth the temperature step and salinity feature. The foregoing evidence for salt fingers indicates a horizontal extent of at least 200 meters, the horizontal extent of these measurements.

TOWED SENSOR MEASUREMENTS OF OCEAN MICROSTRUCTURE

In order to investigate the intensity levels and horizontal spatial variability of ocean microstructure, a

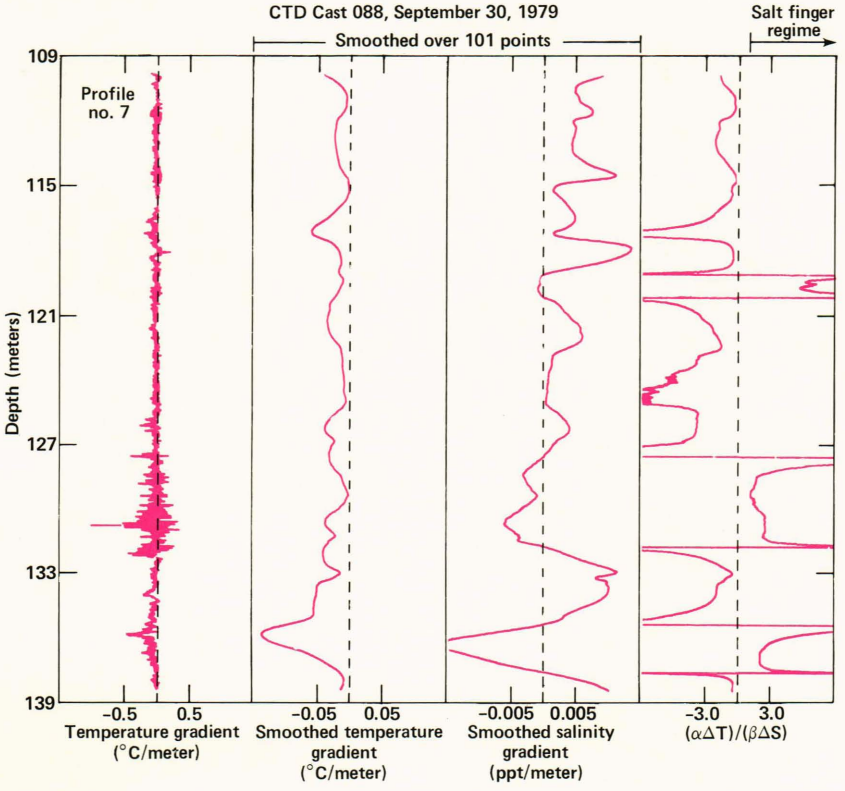

Figure 6 — The temperature gradient ($\Delta T/\Delta Z$) plot for profile no. 7 of Fig. 5 is reproduced along with smoothed temperature and salinity gradient profiles. These smoothed plots (running average over 2 meters) have been used to generate the plot in the fourth panel of stability parameter $\alpha\Delta T/\beta\Delta S$. The intense microstructure patches between 127 and 131 meters are associated with values of the stability parameter between 1 and 2 within the range in which salt fingers are predicted.

set of five fast-response conductivity sensors was built to be used in conjunction with APL's thermistor chain.[14] These sensors were built to APL specifications by NBIS and are shown in Fig. 7 being deployed. The five sensors were separated on the chain by a distance of 3 meters, giving a total aperture of 12 meters.

Conductivity sensors were chosen instead of thermistors to measure temperature[15] because their essentially instantaneous response allows the measurement of very small-scale ($\lambda \approx 1$ centimeter) features at tow speeds of up to 8 knots. To achieve this resolution, a standard NBIS four-electrode conductivity cell was cut down from its standard length of 3 centimeters (as used on the CTD fluorometer system) to 1.5 centimeters, thereby reducing as much as possible the tendency for the cell to average over small-scale features. The effect on the data of the finite (1.5 centimeters) cell length is roughly equivalent to performing a spatial moving average over a length slightly greater than the cell length. This technique leads to a wave-number response function of the form of Eq. 2 as discussed for the CTD fluorometer system. This function is within 3 decibels of unity for wavelengths larger than 4 centimeters; thus, fluctuations with wavelengths greater than 4 centimeters are nominally unattenuated whereas those with smaller scales require significant correction.

Because of the very small amplitudes of short wavelength oceanic conductivity fluctuations, it was necessary to boost the amplitude of the high-frequency signals in the in-water electronics prior to digitization and before transmission up the cable, where noise contamination could occur. This signal conditioning was accomplished by subjecting the conductivity-dependent voltage to a prewhitening filter of the form

$$H(\omega) = 1 + \frac{j\omega\tau_1}{1 + j\omega\tau_2}, \qquad (3)$$

where $\omega = 2\pi f$, and τ_1 and τ_2 are constants. This filter is flat up to $f_1 = 1/2\pi\tau_1 = 1/4$ hertz, where it begins rising at 6 decibels per octave up to $f_2 = 1/2\pi\tau_2 = 200$ hertz, at which point it levels off to constant gain (of f_2/f_1, or 800). This filtering operation allowed the fluctuations occurring in even the less intense patches of microstructure to be measured with a good signal-to-noise ratio nearly out to the system's high-frequency cutoff at 400 hertz.

A fairly typical 900-meter-long tow in the Sargasso Sea that exhibits microstructure activity is shown in Fig. 8. Patches of activity with widths of from several meters up to hundreds of meters are seen by all sensors. However, adjacent sensors do not encounter microstructure simultaneously, indicating that patch heights are usually less than the 3-meter spacing between sensors.

These observations of what appear to be relatively short (about 3 meter) but broad (about 300 meter) patches are consistent with the CTD fluorometer system yo-yo measurements and may also be associated

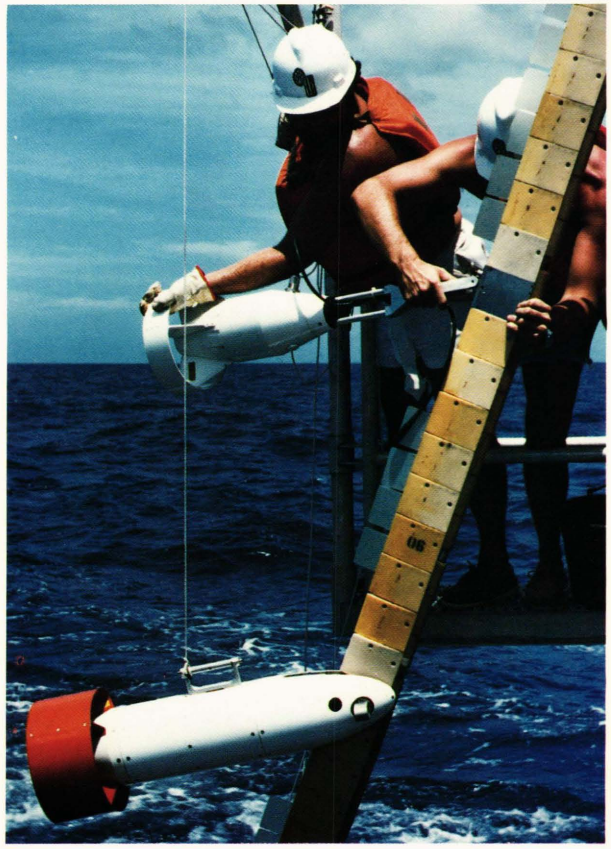

Figure 7 — Sensors being deployed on towed chain. The upper sensor is a fluorometer; the lower is one of the conductivity sensors.

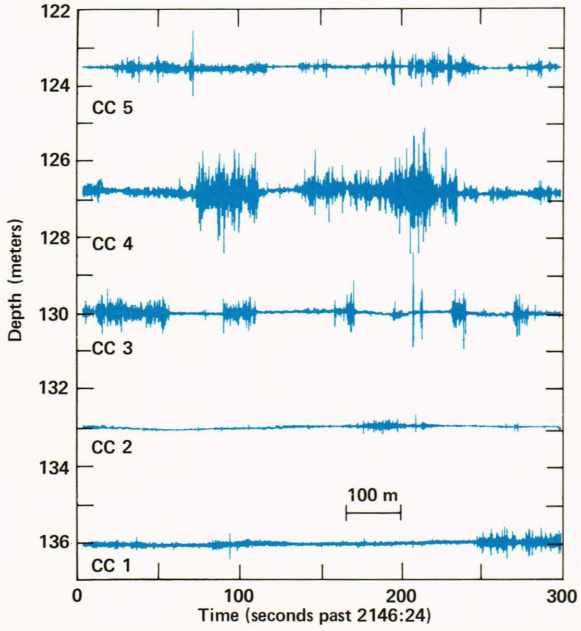

Figure 8 — Fluctuations of conductivity gradient in the wave-number band between 0 and 6 cycles per meter observed during a 900 meter tow in the Sargasso Sea. Tow speed was 3 meters per second. The time scale represents elapsed time past 2146:24 on September 19, 1979. Although microstructure is observed in the top three traces, the lack of simultaneous encounter indicates that the patch heights are less than the 3-meter spacing between the sensors.

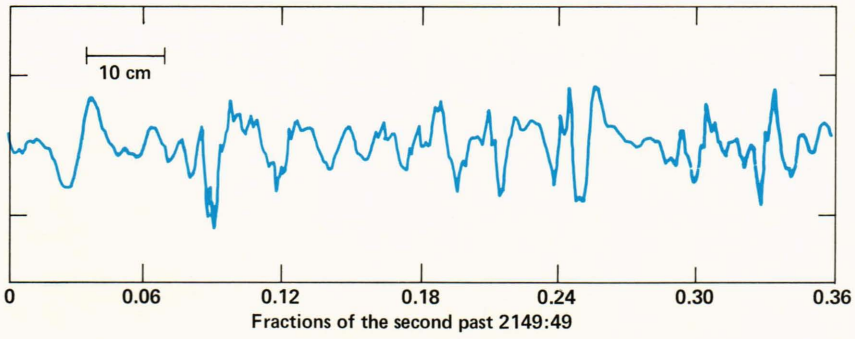

Figure 9 — Plot of conductivity gradient (sensor 4) for a portion (1.1 meters) of the record shown in Fig. 8. Tow speed was 3 meters per second. The smaller scale features have half-widths of 0.5 to 1 centimeter, implying ages between 1 and 3 minutes. Thus, these features appear to be continuously generated over a region less than 3 meters in the vertical. These observations are consistent with either salt fingering or shear instabilities.

with depths unstable to salt fingering. However, there are other mechanisms[16] that can produce patches, such as shear instabilities and internal wave overturning. The lack of joint activity on adjacent sensors does not necessarily mean that the vertical extent of the initial mixing was less than 3 meters, because ambient current shear (du/dz) could destroy the vertical alignment of a tall patch. For example, a typical current shear of 5×10^{-3} meter per second per meter would cause relative horizontal displacements between adjacent sensors of 50 to 100 meters if allowed to act for one hour.

We can test whether the observed horizontal displacement between patches measured by adjacent sensors could be caused by ambient shear, by the following arguments. The maximum length of time the shear has had to act is the age of the patch. This age can be estimated from the relationship[17]

$$\tau = l^2/4K_T \ , \qquad (4)$$

where l is the $1/e$ half-width of a gradient spike, K_T is the thermal diffusivity of water (in this case, 1.5×10^{-3} square centimeter per second), and τ is the age of the spike assuming it had zero thickness at $t = 0$. Figure 9 shows a magnified time series of conductivity gradient from a portion of the record in Fig. 8. The smaller scale gradient features have 1- to 2-centimeter full thickness,[18] implying a half-width of 0.5 to 1 centimeter and ages between 1 and 3 minutes. Even the thicker gradient features have implied ages of approximately 7 minutes. Over these short periods of time, shear displacements between adjacent sensors will only be several meters. Thus, these small-scale features appear to be continuously generated over a region less than 3 meters in the vertical.

As previously mentioned, the horizontal extent of the patches is quite variable, ranging from about 1 to about 300 meters; however, the smaller patches seen primarily in the traces adjacent to the most active trace may actually be part of the bigger patch that they adjoin. Hence, the extremely short duration of these smaller patches may be a result of the intermittence of the upper and lower boundaries of the larger patch and perhaps also may be a result of sensor motion in the vertical.

Thus, these data appear to be consistent with a process of active mixing that occurs over a vertical extent of 1 to 3 meters and several hundred meters in the horizontal. Both shear instabilities and salt fingering associated with unstable regions of the temperature and salinity profiles could account for these properties.

CONCLUDING REMARKS

Measurements of ocean microstructure obtained by using single-point sensors either towed or dropped from a ship give only a one-dimensional view of the ocean. The two-dimensional view of ocean microstructure afforded by the present measurements has allowed the identification of flat patches of large horizontal extent believed to be the result of salt fingering at sites of temperature-stabilized salinity inversions. Because we have only presented a small subset of a data set rather limited in spatial and temporal extent, no conclusions can be drawn regarding how representative these results might be of other ocean areas. But since ocean turbulence is a dissipative process, its characteristics should depend strongly upon the nature of the associated energy sources. Energy sources such as atmospheric forcing, major currents, seasonal heating and cooling, and topography are quite variable in space and time and so, too, should be the characteristics of the resulting turbulence. Currently, the oceanographic community is making rapid progress in discovering the nature and distribution of oceanic turbulence, but we still appear to be far from a comprehensive understanding.

REFERENCES and NOTES

[1] V. T. Neal, S. Neshyba, and W. Denner, "Thermal Stratification in the Arctic Ocean," *Science* **166**, 373-374 (1969).
[2] E. T. Degens and D. A. Ross, eds., *Hot Brines and Recent Heavy Metal Deposits in the Red Sea*, Springer-Verlag, Berlin (1969).
[3] R. I. Tait and M. R. Howe, "Some Observations of Thermo-Haline Stratification in the Deep Ocean," *Deep Sea Res.* **15**, 275-280 (1968).
[4] J. W. Cooper and H. Stommel, "Regularly Spaced Steps in the Main Thermocline Near Bermuda," *J. Geophys. Res.* **73**(18), 5849-5854 (1968).
[5] J. S. Turner, *Buoyancy Effects in Fluids*, Cambridge University Press, Cambridge, England (1973).
[6] M. C. Gregg and M. G. Briscoe, "Internal Waves Finestructure, Microstructure, and Mixing in the Ocean," *Rev. Geophys. Space Phys.* **17** (1), 1524-1548 (1979).
[7] A. J. Williams III, "Images of Ocean Microstructure," *Deep Sea Res.* **22**, 811-829 (1975).
[8] B. Magnell, "Salt Fingers Observed in the Mediterranean Outflow Using a Towed Sensor," *J. Phys. Oceanogr.* **6**, 511-523 (1976).
[9] R. W. Schmitt, Jr. and D. L. Evans, "An Estimate of the Vertical Mixing Due to Salt Fingers Based on Observations in the North Atlantic Central Water," *J. Geophys. Res.* **83**(C6), 2913-2919 (1978).

[10]J. Calman, "Experiments on High Richardson Number Instability of a Rotating Stratified Shear Flow," *Dyn. Atmos. Oceans* **1**, 277-297 (1977).
[11]A. D. Voorhis, D. C. Webb, and R. C. Millard, "Current Structure and Mixing in the Shelf/Slope Water Front South of New England," *J. Geophys. Res.* **81** (21), 3695-3708 (1976).
[12]J. D. Woods, "Wave-Induced Shear Instability in the Summer Thermocline," *J. Fluid Mech.* **32**, 791-800 (1968).
[13]G. S. Keys and B. F. Hochheimer, "The Design of a Simple Fluorometer for Underwater Detection of Rhodamine Dye," *Sea Technol.* **17**(9), 24-47 (1977).
[14]F. F. Mobley, A. C. Sadilek, C. J. Gundersdorf, and S. D. Speranza, "A New Thermistor Chain for Underwater Temperature Measurement," *MTS-IEEE Oceans '76 Conf. Proc.*, pp. 2001-2008 (1976).
[15]Conductivity fluctuations are caused mainly by variations in temperature for many parts of the ocean, with the effects of salinity being small: $(\Delta T/^\circ C) \approx \Delta C(\text{mmho/cm})/1.06$.
[16]M. C. Gregg, "Microstructure Patches in the Thermocline," *J. Phys. Oceanogr.* **10**, 915-943 (1980).
[17]T. R. Osborn and C. S. Cox, "Oceanic Fine Structure," *Geophys. Fluid Dyn.* **3**, 321-345 (1972).
[18]The cell size of 1.5 centimeters prevents observation of gradient features with full widths less than 1.5 centimeters.

ACKNOWLEDGMENT — The authors wish to acknowledge the contributions of Melvin Hennessy and Bryce Troy, who were responsible for the development of computer programs for processing and displaying the data.